Dyes and Pigments 92 (2011) 689–695

Contents lists available at ScienceDirect

Dyes and Pigments

journal homepage: www.elsevier.com/locate/dyepig

Synthesis, crystal structure, optical properties, DNA-binding and cell imaging of an organic chromophore

Shuangsheng Zhou [a,b], Qiong Zhang [a], Xiaohe Tian [c], Guiju Hu [a], Fuying Hao [a], Jieying Wu [a], Yupeng Tian [a,d,e,*]

[a] Department of Chemistry, Key Laboratory of Functional Inorganic Materials Chemistry of Anhui Province, Anhui University, Hefei 230039, PR China
[b] Department of Pharmacy, Anhui College of Traditional Chinese Medicine, Hefei 230031, PR China
[c] Department of Biomedical Science, University of Sheffield, Sheffield, UK
[d] State Key Laboratory of Crystal Materials, Shandong University, Jinan 502100, PR China
[e] State Key Laboratory of Coordination Chemistry, Nanjing University, Nanjing 210093, PR China

ARTICLE INFO

Article history:
Received 19 February 2011
Received in revised form
14 June 2011
Accepted 15 June 2011
Available online 1 July 2011

Keywords:
Organic chromophore
Crystal structure
Optical properties
DNA-binding
Cytotoxicity
Cell imaging

ABSTRACT

An organic chromophore (4-[*N*, *N*- bis(2′-chloroethyl)anilino] ethenyl *N*-methyl pyridinium-*N*- methyl iodide) **L** was synthesized and fully characterized by elemental analysis, IR, ^{1}HNMR spectra and single crystal X-ray diffraction analysis. One and two-photon fluorescence spectra for it were studied. Interestingly, **L** exhibited obvious two-photon absorption in the range from 700–850 nm in DMSO solution. The interactions between the chromophore and calf thymus DNA were investigated by absorption, fluorescence spectra and viscosity experiments. The results showed that the chromophore could interact with DNA in the mode of intercalation and be effectively used as fluorescent staining dye for cell imaging applications. Furthermore, the cell viability data for MCF-7 (Human breast carcinoma) cells indicated that the low-micromolar concentrations of the **L** are essentially non-toxic and can be applied in brighter two-photon fluorescent (TPF) bioimaging.

1. Introduction

Organic chromophores with a large two-photon absorption (TPA) cross section have become of particular interest to chemists and material scientists in decades years due to their potential applications in upconverted lasing [1,2], three-dimensional fluorescence microscopy [3,4], biosensing technology [5,6], optical data storage [7,8], and 3D microfabrication [9,10]. Among these applications, bioimaging as fluorescence probes in living cells has recently attracted a great deal of attention [11–13]. To detect cell imaging in a living system, various fluorescent probes including organic dyes, inorganic nanoparticles, and lanthanide coordination complexes have been developed [11,14,15]. However, recent investigations reveal the most probes with two-photon fluorescence easily exhibit quenching in high polar solvents and TPA maximum not in the near IR range.

Therefore, the challenge before us is how to design and synthesize the chromophores bearing strong two-photon absorption in the near-infrared (NIR) region (bio-safety window) and high polar solvent. For this purpose, the crystal structure, one and two-photon absorption properties, DNA-binding, and cell imaging of a new chromophore **L** which was based on our previous work [16–18] were investigated systematically in this paper.

2. Experimental

2.1. General

The ^{1}H spectra were performed on Bruker 400 spectrometer with TMS as the internal standard, coupling constants J are given in Hertz. Elemental analysis was performed on Perkin–Elmer 240 instrument. Single-crystal X-ray diffraction measurements were carried out on a Bruker Smart 1000 CCD diffractometer equipped with a graphite crystal monochromator situated in the incident beam for data collection at room temperature. The determination of unit cell parameters and data collections were performed with MoK_α radiation ($\lambda = 0.71073$ Å). Unit cell dimensions were obtained with

* Corresponding author. Department of Chemistry, Key Laboratory of Functional Inorganic Materials Chemistry of Anhui Province, Anhui University, Hefei 230039, PR China. Tel.: +86 551 5108151; fax: +86 551 5107342.
E-mail address: yptian@ahu.edu.cn (Y. Tian).

0143-7208/$ – see front matter © 2011 Elsevier Ltd. All rights reserved.
doi:10.1016/j.dyepig.2011.06.021

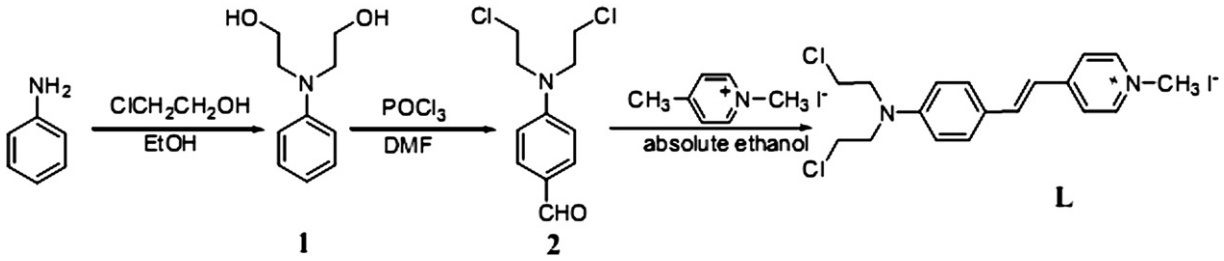

Scheme 1. The synthetic route of the chromophore **L**.

least-squares refinements, and all structures were solved by direct methods using SHELXL-97 [19]. All non-hydrogen atoms were refined anisotropically. The hydrogen atoms were added theoretically and not refined. The final refinement was performed by full-matrix least-squares methods with anisotropic thermal parameters for non-hydrogen atoms on F^2. Fluorescence emission spectra were measured on Perkin–Elmer Lambda-850 spectrophotometer and Perkin–Elmer Ls55 Spectrofluorophotometer, respectively. Tris–HCl buffer (5 mM tris(hydroxymethyl) aminomethane (Tris) hydrochloride, 50 mM NaCl, pH 7.2) was used for absorption titration, emission titration and viscosity experiments. Solutions of DNA(Sigma.Co) in buffer gave a ratio of UV absorbance at 260 and 280 nm of 1.8–1.9:1, indicating that the DNA was sufficiently free of protein [20]. The concentration of DNA was determined spectrophotometrically assuming a molar absorption is 6600 $M^{-1}\,cm^{-1}$ (260 nm) [21].

2.2. Preparation

All chemicals were available commercially and the solvents were purified as conventional methods before using. *N*-phenyldiethanolamine (**1**) was synthesized by the published procedures [18]. The target chromophore **L** was synthesized by following reactions (shown in Scheme 1).

2.2.1. Synthesis of N, N-bis(2-chloroethyl) phenylimino (*2*)

$POCl_3$ (29.2 g, 0.18 mol) was slowly dropped into a dry 100 cm^3 flask which contained 30 g DMF and was cooled with an ice water ahead. The mixture was stirred vigorously while *N*-phenyldiethanolamine (**1**) was added dropwise, the reaction mixture was stirred and refluxed for ca. 16 h at 110 °C, cooled to room temperature, and then the remains was poured into slowly 500 cm^3 ice water. The NaOH solution was added to adjust the pH of the solution under vigorous stirring. After the pH in the solution had reached 7.0, the beige suspension was filtered and fully washed with distilled water three times. The product was dried and recrystallized from EtOH. Beige needle crystals (**2**) were obtained in 88% yield. Mp: 87.6–89.2 °C, ^{1}H NMR($CDCl_3$): δ 9.67(s, 1H, CHO), 6.74–7.38 (m, 4H, Ph), 3.84 (t, $J = 6.8$ Hz, 4H, 2 × NCH_2), 3.68(t, $J = 6.7$ Hz, 4H, 2 × CH_2Cl). Anal. Calcd. for $C_{11}H_{13}Cl_2NO$: C, 53.66; H, 5.32; N, 5.69; found C, 53.42; H, 5.03; N, 5.45.

2.2.2. Synthesis of 4-[N, N- bis(2′-chloroethyl)anilino]ethenyl N-methyl pyridinium iodide (*L*)

The chromophore **2**(4.9 g, 20 mmol) and 1,4-dimethyl pyridinium iodide(4.7 g, 20 mmol) were mixed in 60 mL of absolute ethanol in the presence of 4 drops of piperidine as a catalyst. The resulting mixture was heated to reflux overnight. After cooling, the mixture was filtered to collect the solid followed by washing with ethanol. The crude product was recrystallized twice from ethanol and then dried in vacuo over P_2O_5 to give red crystal (**L**) in 52.3% yield. Mp: 143–145 °C; ^{1}H NMR (DMSO-d_6): δ3.66 (t, $J = 6.7$ Hz, 4H, 2 × CH_2Cl), 3.86 (t, $J = 6.8$ Hz, 4H, 2 × NCH_2), 4.37 (s, 3H, CH_3), 6.43 (d, $J = 2.1$ Hz, 1H), 6.59 (d, $J = 2.1$ Hz, 1H), 6.74–7.38 (m, 8H, 4 × PhH and 4pyridin –H); Anal. Calcd. for $C_{18}H_{21}Cl_2N_2I$: C, 46.66; H, 4.57; N, 6.05; found C, 46.52; H, 4.76; N, 6.21.

2.3. DNA-binding experiments

2.3.1. Absorption measurement

The absorptions of **L** were performed by using a fixed compound concentration to which increments of the DNA stock solution were added. The solutions were allowed to incubate for 10 min before the absorption spectra were recorded. The operation processes were repeated until there was no change for the spectra at least three times, indicating binding saturation had been achieved.

2.3.2. Fluorescence measurement

In the fluorescence quenching experiments, DNA was pretreated with ethidium bromide (EB) for 30 min. The chromophore **L** was

Table 1
Crystal data collection and structure refinement of **L**.

CCDC No	744865
Empirical formula	C36 H44 Cl4 I2 N4 O1
Formula weight	944.35
Crystal system	Monoclinic
Space group	C2/c
a, *b*, *c* (Å)	26.091(5)
	11.736(5)
	17.442(5)
β (°)	128.708(5)
V (Å^3)	4168(2)
Z	4
D_{calc} (g/cm^3)	1.505
F(000)	1880
Crystal size (mm)	0.30 × 0.20 × 0.20
Temperature (K)	298(2)
θ range (°)	2.00–24.99
Total no. of data	16691
No. of unique data	3652
No. of para refined	227
R_1	0.0607
wR_2	0.2099
Gof	1.074

$R(F_o) = \Sigma||F_o| - |F_c||/\Sigma|F_o|$, $R_w(F_o) = (\Sigma w||F_o| - |F_c||^2/\Sigma|F_o|^2)^{1/2}$, $w = [\sigma^2(F_o) + (0.002F_o)^2]^{-1}$.

Table 2
Selected bond lengths (Å) and angles (°) for of **3**.

N_2–C_{12}	1.381(9)
N_2–C_{15}	1.490(11)
N_2–C_{17}	1.465(11)
C_4–C_7	1.452(11)
C_7–C_8	1.316(12)
C_8–C_9	1.471(11)
C_{12}–N_2–C_{15}	121.1(6)
C_{12}–N_2–C_{17}	121.3(6)
C_{15}–N_2–C_{17}	117.4(7)

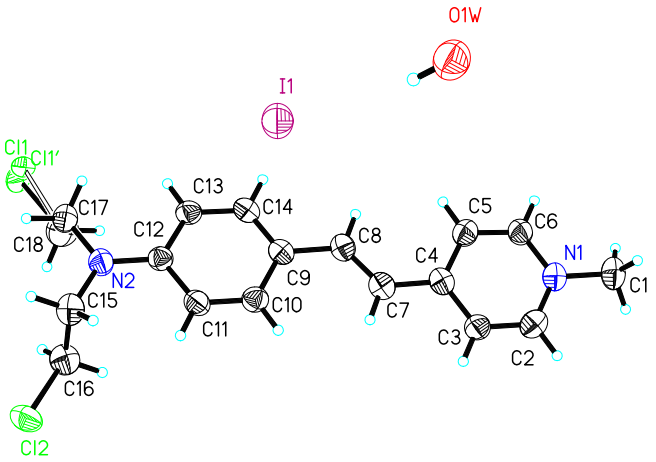

Fig. 1. Molecular structure with atom numbering of **L** showing 50% probability displacement.

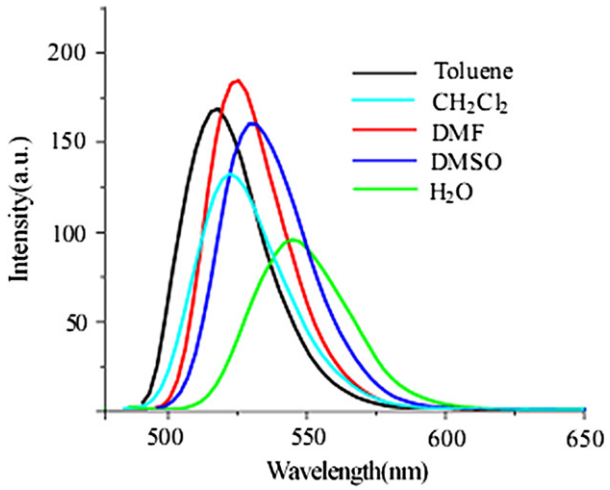

Fig. 3. Sigle-photon fluorescence spectra of **L** in different solvents with 1×10^{-5} mol L^{-1}.

then added to the mixture solution and the effect on the emission intensity was measured by keeping [DNA]/[EB] = 20 ([DNA] = 100 μM, [EB] = 5 μM). Excited at 370 nm, the emission spectra were observed in the range from 450 to 700 nm.

2.3.3. Determination of viscosity

Viscosity measurements were carried out using an Ubbelohde viscometer, immersed in a water bath maintained at 30 ± 0.2 °C. DNA was previously solicited for 30 min, followed by nitrogen bubbling for 5 min. The DNA concentration was kept constant while that of **L** increased. The flow time through the solution were measured three times to get the mean values with a digital stopwatch. The data are presented as $(\eta/\eta_0)^{1/3}$ versus binding ratio ([**L**]/[DNA]), where η and η_0 is the viscosity of DNA in the presence and absence of the chromophore, respectively.

2.4. Cell image and cytotoxicity assay

2.4.1. Cell image

Cells were seeded in 6 well plates at a density of 2×10^4 cells per well and grown for 96 h. For live cell imaging cell cultures were incubated with **L** (10% PBS: 90% cell media) at concentrations 50 μM and maintained at 37 °C in an atmosphere of 5% CO_2 and 95% air for incubation 2 h. The cells were then washed with PBS (3 × 3 ml per well) and 3 ml of PBS was added to each well. The cells were imaged using confocal laser scanning microscopy and water immersion lenses. Excitation energy of 760–800 nm was used and the fluorescence emission measured from 550 nm–650 nm. Co-staining was performed using 5 μM SYTO9, 10 μM PI for 10 min in PBS.

Microscopy: MCF-7 cells were luminescently imaged on a Zeiss LSM 510 META upright confocal laser scanning microscope using magnification 40× and 100× water-dipping lenses for monolayer cultures.

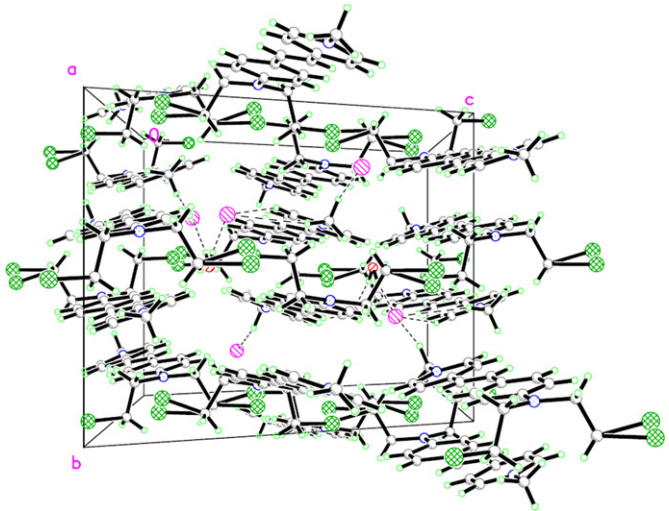

Fig. 2. Packing diagram of **L**.

2.4.2. Cytotoxicity assay

Establishment details of human breast adenocarcinoma cell line (MCF-7) used for cytotoxicity testing in vitro of target derivatives have been previously described [22]. Drug solutions of appropriate concentration were added to a culture containing MCF-7 cells at 2.0×10^4 cells mL^{-1} of medium and the drug exposure was protracted for 24 h. All assays were performed in triplicate, as previously described [22].

3. Results and discussion

3.1. Structure features

The single crystals of **L**, suitable for the X-ray diffraction analysis, were obtained by slow evaporation of acetonitrile at room temperature several days later (Table 1). The selected bond

Table 3
Single- and two-photon-related photophysical properties of chromophore **3** in several different polar solvents.

Solvents	λ_{max}/nm[a]	λ_{max}/nm[b]	λ_{max}/nm[c]	Φ[d]	Δν/cm^{-1}[e]
DMF	426	521	578	0.17	4280
DMSO	425	529	586	0.13	4625
H_2O	427	544	592	0.09	5036

[a] Peak position of the longest absorption band.
[b] Peak position of SPEF, exited at the absorption maximum.
[c] Peak position of the two photon absorption band.
[d] Quantum yields determined by using coumarin as standard.
[e] Stokes shift in cm^{-1}.

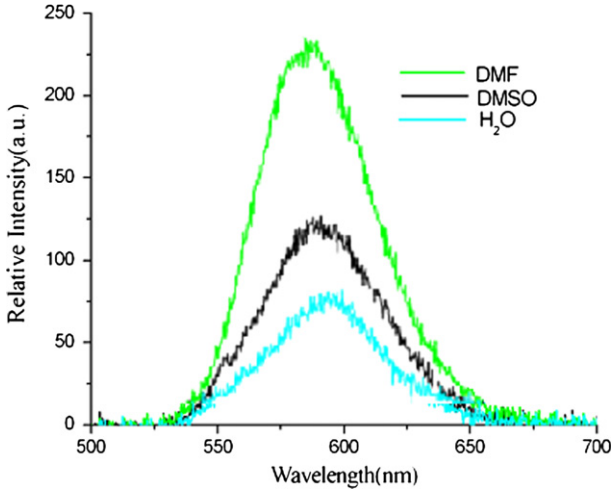

Fig. 4. Two-photon fluorescence spectra of the chromophore **L** in different solvents at a concentration of 1.0×10^{-3} mol L^{-1}.

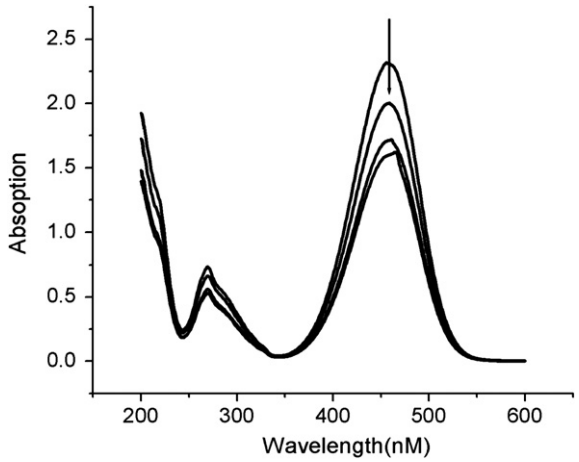

Fig. 6. Absorption spectra of **L** in Tris–HCl buffer (NaCl, PH = 7.2) upon addition of DNA. [compound] = 2×10^{-5} M, [DNA] = (0, 1, 2, 3) $\times 10^{-5}$ M. Arrows show the absorbance changing upon adding DNA concentrations.

distances and angles were listed in Table 2. The structure of **L**, together with the atom numbering scheme was shown in Fig. 1. For the molecular structure of **L**, the least-square plane calculations show that the dihedral angle between the two benzene rings is 8.5, indicating they are nearly coplanar. The sum of the three C–N–C angles taking nitrogen atom as center (C_{12}–N_2–C_{15}, 121.1(6)°; C_{12}–N_2–C_{17}, 121.3(6)°; C_{15}–N_2–C_{17}, 117.4(7)°) is 359.8°, therefore the trigonal NC_3 is practically coplanar. The bond lengths of N_2–C_{15} (1.490(11)) and N_2–C_{17} (1.465(11)) are longer than that of N_2–C_{12} (1.381(9)), confirming the two electrons on N_2 are partial to the adjacent phenyl ring. It can be seen from Table 2 that all the bond lengths of C–C are located between the normal C=C double bond (1.32 Å) and C–C single bond (1.53 Å), which show that there is a highly π- electron delocalized system in the chromophore molecule **L**, which is the necessary condition for it bearing a large TPA cross-section σ [23].

Fig. 2 shows that the adjacent chromophore molecules **L** in the crystal are stacked through strong π–π interactions along *c* axis stacked in pairs through C–H···I interactions.

3.2. Single and two-photon excited fluorescence spectra of *L*

The sigle-photon fluorescence spectra of **L** in five different polar solvents, including aqueous solution (as shown in Fig. 3), and exhibit red shift with increasing of the solvent polarity. The solvatochromism is indicative of a larger stabilization of the excited state than the ground state in a polar solvent, suggesting that a significant charge redistribution takes place upon excitation with consistent of ICT (Intramolecular Charge Transfer) character [16,24].

In order to further demonstrate the influence of solvent on fluorescence, Table 3 lists the Stokes' shift of **L** in three polar solvents. The Stokes' shift is defined as the loss of energy between absorption and reemission of light, which is a result of several dynamic processes. The Lippert equation is the most widely used equation to describe the effects of the physical properties of the solvent on the emission spectra of fluorophores [25].

$$\Delta\nu = \nu_{abs} - \nu_{em} = \left(2/cha^3\right)\Delta f\left(\mu_e - \mu_g\right)^2 + \text{const}$$

where *h* is Planck's constant, *c* is the speed of light, and *a* is the radius of the cavity in which the fluorophore resides. The wavenumbers of the absorption and emission are ν_{abs} and ν_{em} (in cm^{-1}). The Stokes' shifts are approximately proportional to the polarity of the solvent (Table 3).

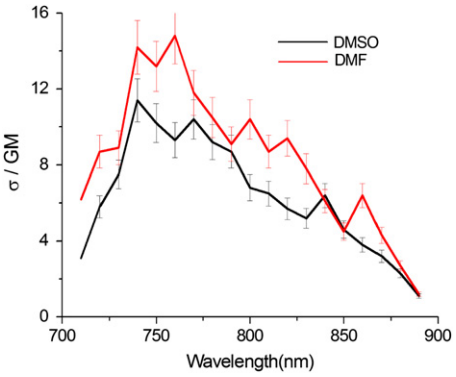

Fig. 5. TPA cross section of **L** in DMF and DMSO *vs* excitation wavelengths.

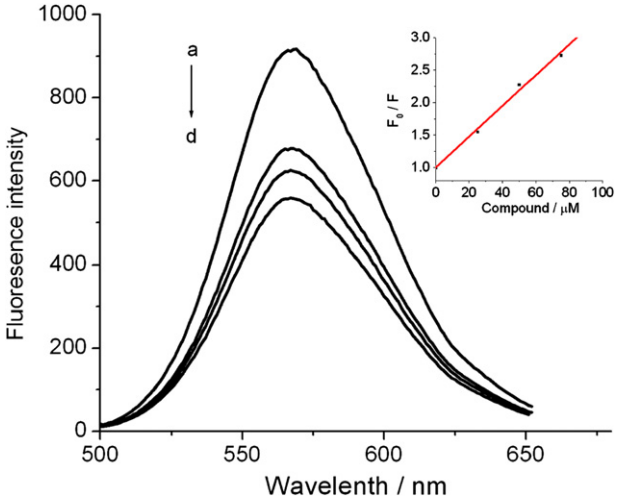

Fig. 7. Fluorescence emission spectra of EB bound to DNA in the absence and presence of different concentrations of compound **L** in Tris–HCl buffer (NaCl, PH = 7.2). [EB] = 5 μM; [DNA] = 100 μM; [compound] = 0 μM (a), 50 μM (b), 100 μM (c), 150 μM (d). Inset: plots of F_0/F versus [compound] for the titration of compound 3 to HS-DNA-EB system.

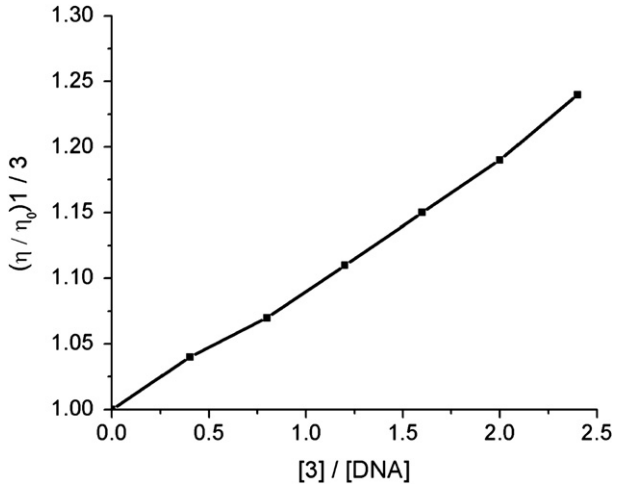

Fig. 8. Effect of increasing concentration of chromophore **L** on the relative viscosities of DNA at 30.0 ± 0.2 °C. [L]/[DNA] = 0.0, 0.4, 0.8, 1.2, 1.6, 2.0, 2.4.

The two-photon excited fluorescence spectra of **L** are shown in Fig. 4 with a solution concentration of 1.0×10^{-3} mol L^{-1} using the optimal excitation wavelength. From Fig. 4, it can be seen that **L** exhibit strong two-photon fluorescence and there is a red shift for the peak position of TPA fluorescence compared with that of single-photon absorption fluorescence due to the reabsorption effect at high concentration [24].

3.3. The TPA cross-section

The two-photon absorption (TPA) cross-section σ was measured by comparing the TPEF intensity of the sample with that of a reference compound by the following equation [26]:

$$\Phi_S = \Phi_r \left(\frac{A_r(\lambda_r)}{A_s(\lambda_s)}\right)\left(\frac{I(\lambda_r)}{I(\lambda_s)}\right)\left(\frac{n_s^2}{n_r^2}\right)\frac{\int F_s}{\int F_r} \quad \sigma_s = \sigma_r F \Phi_r c_r n_r / F_r \Phi_s c n_s$$

Here, Φ is the quantum yield, n is the refractive index, $I(\lambda)$ is the relative intensity of the exciting light, $A(\lambda)$ is the absorbance of the solution at the exciting wavelength λ, and F is the integrated area under the corrected emission spectrum, c is the concentration of the solution in mol L^{-1}. The σ_r value of reference was taken from the literature [16,24]. Subscripts s and r refer to the sample and reference solutions, respectively. The experimental errors are estimated to be ±10% from sample concentrations and instruments. The experimental results show the optimal excitation wavelengths of **L** locate at 740 nm in DMSO and 760 nm in DMF (Fig. 5), the highest cross section values of σ are 11.4 and 14.8 GM (1GM = 10^{-50} cm^4 s $photon^{-1}$), respectively. The wavelengths are suitable for bio-imaging in the near IR range.

3.4. DNA-binding studies

3.4.1. Absorbance titration

The absorption spectra of **L** in the absence and presence of DNA are given in Fig. 6. As the concentration of DNA increased, all the absorption bands of **L** show slightly hypochromism. Such spectral characters suggest that **L** interacts with DNA most likely through a mode involving a stacking interaction between the dye and the base pairs of DNA [27,28].

3.4.2. Fluorescence titration

The emission spectra of EB bound to DNA in the absence and the presence of **L** are given in Fig. 7. The addition of the chromophore **L** to DNA pretreated with EB causes obvious decrease in the emission intensity, indicating that the DNA bound EB fluorophore is partially replaced by the target molecule **L**. The result suggests that **L** presumably intercalate into DNA. According to the classical Stern–Volmer equation [29]:

$$F_0/F = 1 + K[Q]$$

where F_0 and F are of fluorescence intensities in the absence and presence of the compound, respectively. K is a linear Stern–Volmer quenching constant. [Q] is the concentration of the quencher compound. The fluorescence quenching curve (inset in Fig. 7) illustrates that the fluorescence quenching of DNA − bound EB system mixing with **L** is good agreement with the linear Stern–Volmer equation. In the plot of F_0/F versus [L], K is given by the ratio of the slope to intercept. The values of K for **L** is 3.24×10^3 ($R = 0.99629$), which also supports the intercalation of **L** to the ctDNA bases ($K \geq 1.0 \times 10^3$) [27,30].

3.4.3. Viscosity studies

Fig. 8 reveals that the viscosity of DNA is affected significantly by the addition of **L**. The results suggest that the title chromophore intercalates between the base pairs of DNA [28,31], in agreement with the above spectra experimental results.

3.5. Cell image and cytotoxicity assay

To examine the live cellular image properties of the chromophore **L** for two-photon microscopy (TPM), MCF-7 (human breast

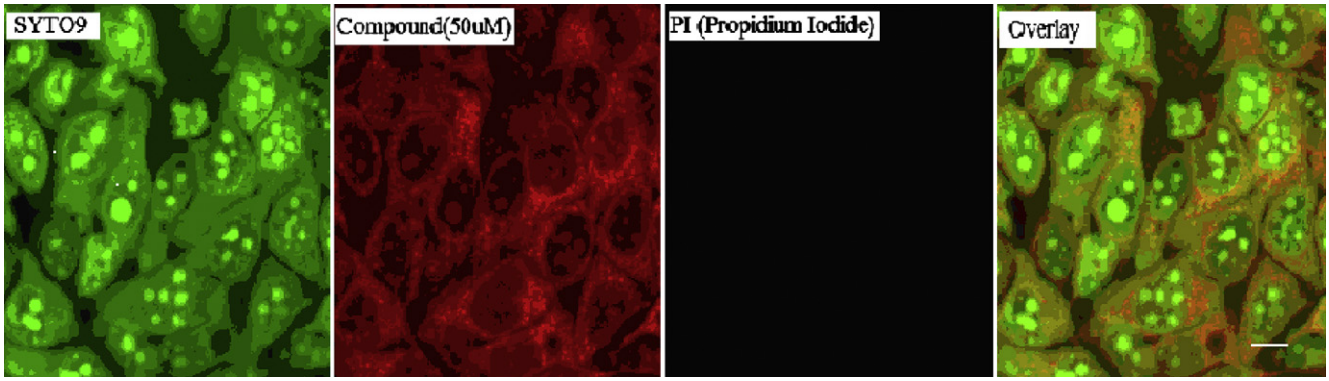

Fig. 9. Chromophore **L** (red, 2 h) with Live/Dead staining by using SYTO9 (green)/Propidium Iodide(PI) and overlay image (the scale bar represents 10 μM) (For interpretation of the references to color in this figure legend, the reader is referred to the web version of this article.).

Table 4
Cell viability (%) of MCF-7 cells after incubation for 24 h with different concentration of the chromophore 3.[a]

Concentration (μM)	5	10	20	40	80
Viability (%)	97.14 ± 1.23	88.43 ± 1.52	73.56 ± 1.46	58.27 ± 1.64	40.06 ± 1.28

[a] Cell viability was quantified by the MTT assay ($n = 3$, mean ± s).

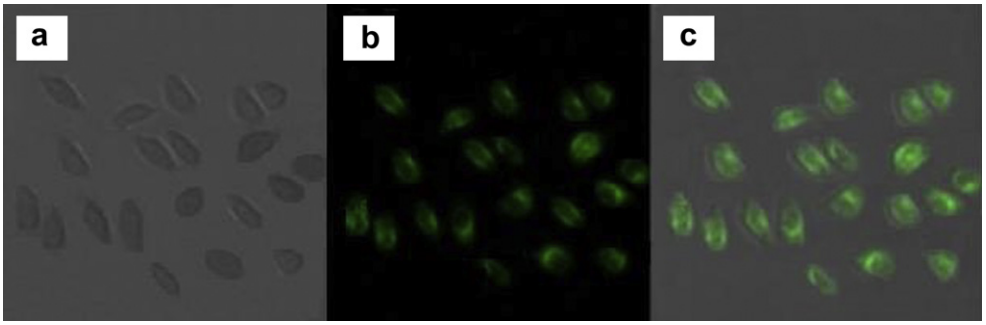

Fig. 10. (a) The bright-field image of MCF-7 cells incubated with 5 μM **L**. (b) Two-photon microscopy (TPM) image of the same cells with excitation at 780 nm. (c) Overlay image.

carcinoma) cells were incubated and stained with 50 μM **L** by co-stain with two commercially available dye-SYTO9 and Propidium Iodide (PI), which perform as cell-permeable nuclear acid dye in live cells and non-cell-permeable DNA dye in dead cells respectively for live/dead staining. After 2 h incubation, the cells was washed by PBS (phosphate buffer solutions) three times and directly move to two-photon microscopy without fixation. As seen from Fig. 9, greenchannel from SYTO9 (left) and purple channel from PI (middle) indicated almost all the cells keep healthy even suffering long incubation time and high concentration. The red channel clearly reveal MCF-7cells successfully uptake **L**, interestingly, the luminescence located in cell cytosol as well as cell nuclear. The luminescences which come from the cytosol suppose that the chromophore permeated the phospholipids bilayers of cellular mitochondria and bounded with mitochondrial DNA hence fluorescence come out eventually. The cellular image result demonstrated that **L** would be able to functionalize as cellular DNA that both exist in cell nuclear and mitochondria.

Cytotoxicity is a potential side effect of **L** that must be controlled when dealing with living cells or tissues. We have conducted cytotoxicity assays in MCF-7 cells before microscopy studies. Table 4 lists the cell viability data for MCF-7 cells treated with **L** as quantified by the MTT assay. These data indicated that MCF-7 cells show nearly ~100% viability following 24 h of treatment with 5 μM **L** (Table 4). Although obvious decrease of cell viable was observed when incubated reach high concentration. These cytotoxicity tests showed that sub- and low-micromolar concentrations of **L** are essentially nontoxic over a period of 24 h and could safely be used for further biological studies.

To further demonstrate the potential applications of **L** for two-photon microscopy (TPM) imaging in living cells, MCF-7 cells were cultured and stained with **L**. A bright-field image (Fig. 10a) of each cell was taken immediately prior to the two-photon microscopy (TPM) imaging. The results showed that **L** is clearly capable of detecting the cytoplasm section in MCF-7 cells. The record TPA coefficient of **L** and its application for in vivo two-photon imaging highlight the potential of the chromospheres (Fig. 10b, c).

4. Conclusions

An organic chromophore **L** has been synthesized and characterized by single crystal X-ray diffraction analysis. Interestingly, **L** exhibits strong two-photon excited fluorescence intensity in the near IR range in DMSO solution and can obviously interact with DNA *via* intercalating interaction as well. Significantly, **L** exhibits brighter two-photon fluorescent bioimaging which make it successfully applied to a two-photon fluorescent staining dye in live cells. Further work involving co-localization fluorescence study and 3D cell image are in progress. These explorations for the chromophore may provide a useful guide to the design of novel TPA materials.

Acknowledgments

This work was supported by a grant for the National Natural Science Foundation of China (21071001, 50873001, 20875001), Department of Education Committee of Anhui Province (KJ2010A030, KJ2010A222), and the Foundation for Scientific Innovation Team of Anhui Province (2006KJ007TD). The 211 Project of Anhui University, Ministry of Education funded projects focus on retired overseas scholar.

References

[1] He GS, Tan LS, Zheng QD, Prasad PN. Multiphoton absorbing materials: molecular designs, characterizations, and applications. Chemical Reviews 2008;108:1245–330.
[2] Lin TC, Hsu CS, Hu CL, Chen YF, Huang WJ. Synthesis and two-photon properties of a multipolar chromophore containing indenofluorenyl units. Tetrahedron Letters 2009;50:182–5.
[3] Lee KS, Kim RH, Yang DY, Park SH. Advances in 3D nano/microfabrication using two-photon initiated polymerization. Progress in Polymer Science 2008; 33:631–81.
[4] Imanishi Y, Lodowski KH, Koutalos Y. Two-photon microscopy: shedding light on the chemistry of vision. Biochemistry 2007;46:9674–84.
[5] Jiang YH, Wang YC, Hua JL, Tang J, Li B, Qian SX, et al. Multibranched triarylamine end-capped triazines with aggregation induced emission and large two-photon absorption cross-sections. Chemical Communication 2010;46: 4689–91.
[6] Wang B, Wang YC, Hua JL, Jiang YH, Huang JH, Qian SX, et al. Starburst triarylamine donor–acceptor–donor ouadrupolar derivatives based on cyano-substituted diphenylaminestyrylbenzene: tunable aggregation-induced emission colors and large two-photon absorption cross sections. Chemistry an European Journal 2011;17:2647–55.
[7] Cheng LH, Li L, Sun PP, Zhou HP, Tian YP, Tang HH. Synthesis, structure and nonlinear optical properties of two novel two-photon absorption chromophores. Science China Chemistry (Series B) 2009;52(4):529–34.
[8] Corredor CC, Huang ZL, Belfield KD, Morales AR, Bondar MV. Photochromic polymer composites for two-photon 3D optical data storage. Chemistry of Materials 2007;19:5165–73.
[9] Zhou W, Kuebler SM, Braun KL, Yu T, Cammack JK, Ober CK, et al. An efficient two-photon-generated photoacid applied to 3D microfabrication. Science 2002;296:1106–9.

[10] Pawlicki M, Collins HA, Denning RG, Anderson HL. Two-photon absorption and the design of two-photon dyes. Angewandte Chemie International Edition 2009;48:3244–66.
[11] Kim MK, Lim CS, Hong JT, Han JH, Jang HY, Kim HM, et al. Sodium-ion-selective two-photon fluorescent probe for in vivo imaging. Angewandte Chemie International Edition 2010;49:364–7.
[12] Lee JH, Lim CS, Tian YS, Han JH, Cho BR. A two-photon fluorescent probe for thiols in live cells and tissues. Journal of the American Chemical Society 2010; 132:1216–7.
[13] Law GL, Wong KL, Cornelia Man WY, Wong WT, Tsao SW, Michael HWL, et al. Emissive terbium probe for multiphoton in vitro cell imaging. Journal of the American Chemical Society 2008;130:3714–5.
[14] Kim HM, Cho BR. Two-photon probes for intracellular free metal ions, acidic vesicles, and lipid rafts in live tissues. Accounts Chemical Research 2009; 42(7):863–72.
[15] Kim HM, Cho BR. Two-photon materials with large two-photon cross sections. Structure-property relationship. Chemical Communication; 2009:153–64.
[16] Hao FY, Zhang XJ, Tian YP, Zhou HP, Li L, Wu JY, et al. Design, crystal structures and enhanced frequency-upconverted lasing efficiencies of a new series of dyes from hybrid of inorganic polymers and organic chromophores. Journal of Materials Chemistry 2009;19:9163–9.
[17] Lei H, Huang ZL, Wang HZ, Tang XJ, Wu LZ, Zhou GY, et al. Two-photon absorption spectra of new organic compounds. Chemical Physics Letters 2002; 352:240–4.
[18] Hao FY, Shi PF, Wu JY, Yang JX, Tian YP, Zhou GY, et al. Synthesis, characterization and two-photon absorption properties of a novel pyridinium salt. Chinese Journal of Chemistry 2004;22:354–9.
[19] Sheldrick GM. SHELXS97 and SHELXS-97. Göttingen: University of Göttingen; 1997.
[20] Temerk YM, Ibrahim MS, Kotb M. Voltammetric and spectroscopic studies on binding of antitumor morin. morin–Cu complex and morin–β–cyclodextrin with DNA. Spectrochimica Acta Part A 2009;71:1830–6.
[21] Hassan MT, Mahboube IM, Adeleh D, Saboury AA. 2, 2′-Bipyridinebutyl dithiocarbamatoplatinum(II) and palladium(II) complexes: synthesis, characterization, cytotoxicity, and rich DNA-binding studies. Bioorganic & Medicinal Chemistry 2008;16:9616–25.
[22] Gao YH, Wu JY, Li YM, Sun PP, Zhou HP, Yang JX, et al. A sulfur-terminal Zn(II) complex and its two-photon microscopy biological imaging application. Journal of the American Chemical Society 2009;131:5208–13.
[23] Zhou HP, Li DM, Wang P, Cheng LH, Gao YH, Zhu YM, et al. Synthesis, crystal structures, and two-photon absorption properties of dithiocarbazate Zn(II) and Pd(II) complexes. Journal of Molecular Structure 2007;826:205–10.
[24] Li L, Tian YP, Yang JX, Sun PP, Wu JY, Zhou HP, et al. Facile synthesis and systematic investigations of a series of novel bent-shaped two-photon absorption chromophores based on pyrimidine. Chemistry an Asian Journal 2009;4:668–80.
[25] Lakowicz JR. Principles of fluorescence spectroscopy. New York: Plenum Press; 1983. p. 190.
[26] Zhou HP, Li DM, Zhang JZ, Zhu YM, Wu JY, Hu ZJ, et al. Crystal structures, optical properties and theoretical calculation of novel two-photon polymerization initiators. Chemical Physics 2006;322:459–70.
[27] Li J, Wei YL, Guo LM, Zhang CH, Jiao Y, Shuang SM, et al. Study on spectroscopic characterization of Cu porphyrin/Co porphyrin and their interactions with ctDNA. Talanta 2008;76:34–9.
[28] Chen LM, Liu J, Chen JC, Shi S, Tang CP. Experimental and theoretical studies on the DNA-binding and spectral properties of water-soluble complex $[Ru(MeIm)_4(dpq)]2+$. Journal of Molecular Structure 2008;881:156–66.
[29] Ling X, Zhong WY, Huang Q, Ni KY. Spectroscopic studies on the interaction of pazufloxacin with calf thymus DNA. Journal of Photochemistry and Photobiology B: Biology 2008;93:172–6.
[30] Liu ZQ, Li YT, Wu ZY, Zhang SF. $[Cu_4(H_2O)_4(dmapox)_2(btc)]_n \cdot 10nH_2O$: the first two-dimensional polymeric copper(II) complex with bridging L – trans-oxamidate and μ4-1,2,4,5-benzentetracarboxylato ligands: synthesis, crystal structure and DNA binding studies. Inorganica Chimica Acta 2009; 362:71–7.
[31] Maribel N, Efren CF, Mercedes FM, Dwight A, Edgar M. Synthesis, characterization, DNA binding study and biological activity against leishmania mexicana of $[Cu(dppz)]BF_4$. Journal of Inorganic Biochemistry; 2003:97364–9.